Protection from oxidation of second and third generation TiAl intermetallic alloys by magnetron sputtering deposition of a TiAl/TiAlN coating

Materials & Design 208 (2021) 109905

Contents lists available at ScienceDirect

Materials & Design

journal homepage: www.elsevier.com/locate/matdes

Protection from oxidation of second and third generation TiAl intermetallic alloys by magnetron sputtering deposition of a TiAl/TiAlN coating

O. Ostrovskaya [a,*], C. Badini [a], S.M. Deambrosis [b], E. Miorin [b], S. Biamino [a], E. Padovano [a]

[a] Polytechnic of Turin, Dpt. Applied Science and Technology – DISAT, C.so Duca degli Abruzzi, 24-10129 Torino, Italy
[b] National Research Council – CNR, Institute of Condensed Matter Chemistry and Technologies for Energy – ICMATE, Corso Stati Uniti, 4 - 35127 Padova, Italy

HIGHLIGHTS

- TiAl-TiAlN coating was deposited on advanced TiAl alloys for oxidation protection.
- Oxidation behaviour was investigated by a burner rig apparatus.
- The coating greatly improved the oxidation resistance up to 1000 °C.
- Passive alumina layer formed on the oxidized surface.
- Performance of the TiAl-TiAlN coating depended on the kind of intermetallic alloy.

GRAPHICAL ABSTRACT

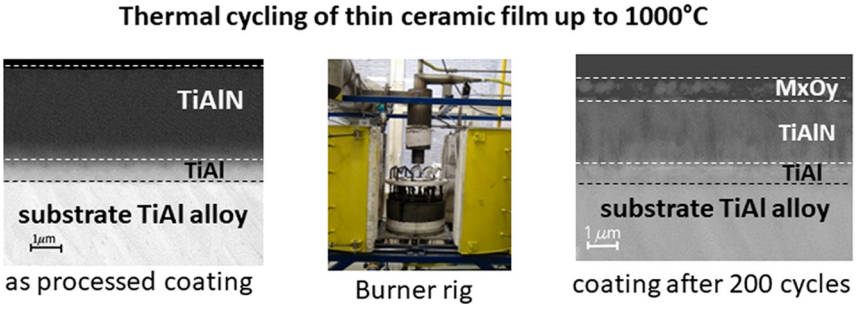

ARTICLE INFO

Article history:
Received 11 January 2021
Revised 1 June 2021
Accepted 15 June 2021
Available online 16 June 2021

Keywords:
A. Films
B. Oxidation resistance
C. Thermal shock resistance
D. Nitrides

ABSTRACT

A two-layer TiAl/TiAlN coating was deposited by High Power Impulse Magnetron Sputtering on the surface of three TiAl intermetallic alloys for improving their oxidation resistance. The effectiveness of the surface coatings was tested in a facility designed for simulating the service conditions of turbine engines components. The response of uncoated and coated samples was compared during thermal cycling up to 1000 °C under oxidizing environment. The growth of oxide layers and the degradation of the coatings were investigated by X-ray Diffraction, Scanning Electron Microscopy, Energy Dispersive X-ray Spectroscopy and X-ray Photoelectron Spectroscopy. The surface coating was found to greatly improve the oxidation resistance of Ti-47Al-2Cr-8Nb and Ti-43.5Al-4Nb-1Mo alloys, while more limited benefits were observed for the Ti-48Al-2Nb-0.7Cr-0.3Si alloy. The different performance of the same coating deposited on different substrates has been tentatively attributed to the different alloying elements present in the intermetallic substrate, and that can diffuse towards the protective coating and the growing oxide layer.

1. Introduction

Intermetallic Titanium Aluminides have been recognized as very attractive lightweight materials for applications at high temperatures in aeronautic and automotive engineering [1–4]. In fact, they show potential for applications in turbines for aircrafts or powerplants, as well as in turbocharger rotors of car engines, owing to their exceptional combination of specific strength and elastic modulus, creep and fatigue behavior. Among the TiAl alloys, the most widely investigated was the Ti-48Al-2Cr-2Nb one, which to date is currently used in fabrication of blades for low-pressure turbines of GEnx (General Electric) and LEAP (SNECMA) jet engines [3,4]. More recently, Pratt&Withney used a novel forgeable

* Corresponding author.
E-mail address: oxana.ostrovskaya@polito.it (O. Ostrovskaya).

https://doi.org/10.1016/j.matdes.2021.109905
0264-1275/

Ti-43.5Al-4Nb-1Mo-0.1B alloy (TNM) in the low pressure turbine of new geared turbofan (GTF) engine [4]. However, these promising TiAl intermetallics still show some lacks dealing with their poor ductility at room temperature, the deterioration of creep behaviour and their poor oxidation resistance at temperature above 850 °C [4]. Advances were achieved by better controlling the alloy microstructure through the use of alloying elements and by improving the manufacturing process and the final thermal treatments of intermetallic components [5]. As a consequence, the TiAl alloys of second and third generation show rather complex compositions, since combinations of many alloying elements (Cr, Mn, Nb, Ta, W, Mo, Hf, Zr, B, C, Si, and rare earths) have been proposed [4]. In particular, the addition of Nb and Mo has been adopted to enhance ductility, creep resistance and service temperature. Several alloying elements (Nb, Mo, Si, W, Zr) are believed to enhance the oxidation resistance too [2,6–9]. Owing to these improvements alloys of third generation, like Ti-43.5Al-4Nb-1Mo and Ti-47Al-2Cr-8Nb, show better oxidation resistance than the most widely used Ti-48Al-2Cr-2Nb alloy [10]. Nonetheless, both mechanical behaviour and oxidation resistance should be further enhanced for using these materials in the hottest parts of engines, and possibly for substituting nickel superalloys for this application.

A very effective approach for improving oxidation resistance of Ti-Al alloys is provided by surface engineering. Several surface coatings and deposition processes have been proposed and tested for this purpose [11–20]. The surface coatings for TiAl intermetallic alloys were designed with the aim of hindering the formation of titanium oxide and promoting the formation of alumina (or of a mixture of Al, Cr and Si oxides) instead [13,15–17]. Actually, alumina shows a passivating behaviour that can greatly limit the growth rate of the oxide scale. Overlay coatings, diffusion coatings, enamel coatings and surface enrichment of fluorine were investigated for the oxidation protection of TiAl alloys [13]. Overlay coatings were deposited by exploiting several techniques: plasma spraying [13,21] and physical vapour deposition by magnetron sputtering [13,14], reactive arc [13,22], and electron beam PVD [13,23]. Diffusion coatings were processed by pack cementation (aluminizing) giving an aluminium rich external layer [13,24]. Unfortunately, several of these coatings (overlay MCrAlY coatings, enamel glassy coatings, aluminized layers based on $TiAl_3$ phase and alumina coatings) failed at high temperature (900–1000 °C) because of crack formation or layer spallation [13]. The failure was attributed to the lack of chemical and thermal expansion compatibility between the oxide layer, the coating and the intermetallic substrate. On the contrary, fairly good oxidation resistance was achieved at 900–950 °C when using Ti-Al-Cr coatings deposited by unbalanced magnetron sputtering on Ti-48Al-2Cr-2Nb, TNM-B1 and Ti-45Al-8Nb alloys [15–17] or using a Ti-Al-Cr-Zr layer deposited on TNB-V2 alloy [18]. In fact, the $Ti(Cr,Al)_2$ Laves phase present inside these coatings was found to promote preferentially the formation of alumina. Rather good results were also achieved by fluorination, but difficulties still remain for practically exploiting this method for the protection of parts with complex shapes [13]. Presently, further efforts should be spent for developing protective coatings suitable to operate over 900 °C. Nitride coatings could be investigated to this purpose. According to first investigations, nitride coatings based on TiAlCrN seemed not suitable for applications above 850 °C [17], while a two-layers protection system comprising a TiAl interlayer and an external TiAlN coating appreciably enhanced the oxidation resistance at 950 °C of Ti-48Al-2Cr-2Nb [19,20]. This protection system processed by reactive high power impulse magnetron sputtering (R-HiPIMS) not only promotes the formation of alumina on the top of the oxide layer but also shows improved toughness and adherence to metallic substrates [25,26], which hinder coating spallation. In fact, TiAlN shows a thermal expansion coefficient (average value between 200 °C and 600 °C = 8.2 10^{-6} K^{-1} [27]) similar to that of Ti-47Al-1.5(Nb,Cr,Si) alloys (10.5 10^{-6} K^{-1} in the 200–600 °C range [28]). Therefore, it would be worthwhile to investigate also its suitability for oxidation protection of TiAl alloys of second and third generation, designed for operating at higher temperature than Ti-48Al-2Cr-2Nb. The present work is aimed to check the effectiveness of the TiAl/TiAlN coating for improving the oxidation behaviour of the alloy of second generation Ti-48Al-2Nb-0.7Cr-0.7Si (RNT), and that of the alloys of third generation Ti-43.5Al-4Nb-1Mo (TNM) and Ti-47Al-2Cr-8Nb (HNb).

These alloys were coated by reactive High Power Impulse Magnetron Sputtering (R-HiPIMS) and their oxidation behaviour was compared with that of uncoated alloys. As previously reported in [19,20] with respect to traditional magnetron sputtering techniques, HiPIMS plasma conditions greatly enhance the flux of energetic ionized species towards the growing film, allowing smoother and denser coatings to be deposited on complex-shaped substrates [29].

Testing was performed in a burner rig heated by methane combustion and specifically designed for simulating the atmosphere inside the turbines of jet engines. The combustion was carried out using air in excess with respect to the stoichiometry of the combustion reaction (lambda coefficient 1.2), thus granting the presence of free oxygen. Moreover, in this apparatus the atmosphere, resulting from fuel combustion, contained combustion products, like water vapour, that could concur with oxygen to the corrosion-oxidation process. Very severe thermal cycles were performed by quickly heating the samples up to 1000 °C and quenching them by an air flow, thus simulating the effect of thermal shocks that could give rise to elastic stresses and promote spallation or cracking of the protective coating.

2. Materials and methods

2.1. Materials

In this work, the effectiveness for oxidation protection of TiAl-TiAlN thin ceramic coatings deposited on different TiAl alloys was studied. The intermetallic alloys Ti-48Al-2Nb-0.7Cr-0.3Si (RNT), Ti-43.5Al-4Nb-1Mo (TNM) and Ti-47Al- 2Cr-8Nb (HNb) were coated with this double layer thin film. Bars of these intermetallic alloys were produced by electron beam melting (EBM) and then thermally treated to modify their microstructure and improve the mechanical behaviour. As a consequence of the thermal treatment the Ti-47Al- 2Cr-8Nb (Ti-30.4Al-2.5Cr-17.8Nb wt. %) and Ti-48Al-2Nb-0.7Cr-0.3Si (Ti-33.5Al-4.8Nb-0.9Cr-0.2Si wt. %) alloys showed a near lamellar microstructure, while the microstructure of Ti-43.5Al-4Nb-1Mo alloy (Ti-28.6Al- 9.1Nb-2.3Mo wt.%) consisted of lamellar γ/α_2 colonies with globular β_0 and γ grains at the grain boundaries [10]. More information about the EBM process and the heat treatments of the TiAl alloys under investigation were reported in previous papers [10,30,31].

2.2. Coating deposition

Cylindrical samples (20 mm high, 15 mm in diameter) were cut from the bars and their circular sections were polished by abrasive paper and diamond pastes to 1 μm surface finishing. Before the film deposition, the samples were cleaned by ultrasound in acetone bath for 20 min, and then gently etched by ion sputtering for two minutes.

A reactive HiPIMS system was used for the surface etching and the subsequent thin films depositions. The system was power supplied by a TRUMPF-Hüttinger - True Plasma High Pulse 4002 unit, coupled with a TRUMPF-Hüttinger – 18 kW special unit model

3018 HBP, specifically designed for substrate biasing with HiPIMS. The high-vacuum chamber was evacuated prior to the depositions by a turbo-molecular pump to a base pressure lower than 1×10^{-5} Pa. A gentle plasma etching was performed under the following conditions: Ti 50% - Al 50% target (~10 cm in diameter, 6 mm thick, 99.9% purity) fixed on a weekly unbalanced magnetron cathode, distance between sample surface and target 100 mm, Ar as working gas (99.9997% purity, 100 sccm, 1 Pa), average cathode power 35 W, frequency 500 Hz, pulse length 35 μs, set temperature 400 °C, substrate bias voltage −1200 V. The substrate heater is made of an array of 8 halogen lamps (250 W, 24 V DC). Two type K thermocouples are placed as close as possible to the samples. The control system used allows one or more lamps to be turned on/off automatically to keep the substrate temperature constant during the process.

In order to improve the adhesion between the substrate and the TiAlN coating, a TiAl interlayer was deposited on the surface of TiAl alloys. The 10 cm diameter TiAl target (1:1) was used for the TiAl interlayer deposition too. The film was obtained under the following conditions: sample surface-target distance 100 mm, gas Ar (working pressure 1 Pa), average power 1000 W, frequency 500 Hz, pulse length 35 μs, temperature 400 °C, substrate bias voltage −60 V, duration 10 min. Using these process parameters, the target peak current density turned out to be 1.5 A/cm^2.

Then, the TiAlN surface layer was deposited using the same Ti 50% - Al 50% target in a mixture of inert gas (Ar) and reactive gas (N_2, 99.998% purity). The mixture of Ar and N_2 (1:1 vol ratio) was introduced through dedicated mass flow controllers. The TiAlN film was obtained under the same sputtering conditions (pressure, average power, frequency, pulse time, temperature and substrate voltage) previously adopted for the glue layer deposition, but with a peak current density equal to 2.8 A/cm^2 and a sputtering duration of 180 min.

2.3. Oxidation resistance investigation

The oxidation resistance of uncoated and coated samples was compared by testing them in a burner rig apparatus, designed for simulating the operating conditions of several components of turbine engines. In this work, all the samples were submitted contemporaneously to oxidation while changing cyclically the temperature up to 1000 °C. A maximum temperature well over the current service temperature of low pressure turbine of jet engines and severe thermal shocks were adopted in view of possible application of advanced TiAl alloys in hotter parts of turbine engines. The burner was fed by a methane/air mixture using 20% of air in excess with respect to the stoichiometry of the combustion reaction. Each thermal cycle consisted of a rapid heating up to 1000 °C (9 min), a two minutes long isothermal step at this temperature, and a final air-quenching to 300 °C (quenching rate 470 °C/min).

The flow of oxygen and methane was calibrated by mass flow controllers, the temperature of each specimen was constantly measured by thermocouples, all data were continuously recorded by the acquisition system and used by the control system for adjusting the experimental conditions according to the designed thermal cycle. More details about the burner rig apparatus were reported in previous papers [19,20]. The microstructure and the thickness of the ceramic coatings deposited on different TiAl substrates were checked before and after thermal cycling (100 and 200 cycles) by electronic microscopy (SEM-EDS), X-ray photoelectron spectroscopy (XPS) and X-ray diffraction (Bragg-Brentano XRD). Before these analyses, the samples were cleaned by ultrasounds in an acetone bath for 20 min. Discs with diameter of 15 mm and thickness of 4 mm were taken from the cylindrical samples after oxidation in burner rig. These samples were used for both XRD and XPS analyses. Cross sections of these discs, surface polished with diamond pastes to obtain 1 μm surface finishing, were used for SEM-EDS analyses.

The composition of both coatings and oxide layers were investigated by SEM-EDS (SEM-FEG Assing SUPRA 25, Oberkochen, Germany, equipped with EDS Oxford INCA X-sight), and the crystalline phases here present were identified by XRD using Cu Kα radiation (Panalytical X'PERT PRO PW3040/60, Panalytical BV, Almelo, The Netherlands).

X-ray Photoelectron Spectroscopy (XPS, PHI 5000 Versa Probe, Chanhassen, MN, USA) was used for investigating the chemical compositions of sample surfaces after oxidation. Experimental results were analysed (for spectra fitting and deconvolution) by Multipack 9.6 software. The fits were obtained using the following curve fit parameters: Shirley background subtraction in the range of binding energy involved in the fitting; 60% Gaussian-40% Lorentzian ratio. X-ray Photoelectron Spectroscopy (XPS) Reference Pages and literature reports were adopted as databases. Survey and high-resolution XPS spectra were obtained after cleaning the sample surface by sputtering in the XPS chamber (Ar + source, 2 kV ions accelerating voltage, 10 μA ion current, sputtering time up to 10 min). It was found that it is necessary to perform step by step this treatment to remove organic surface pollutants coming from sample handling, which otherwise would affect the analysis results. The sputtering was carried out until the C_{1s} peak intensity in the XPS spectra became negligible (carbon content becomes less than 1% after about 10 min of sputtering).

Calibration of XPS apparatus was performed by matching the literature binding energy values of Au 4f7/2, Cu 2p3/2 and Ag 3d5/2 peaks.

3. Results and discussion

3.1. Investigation of composition by XRD analysis

The phases present inside the microstructure of the uncoated and coated alloys were investigated by XRD before and after the oxidation tests. The crystalline phases were identified by using the Joint Committee on Powder Diffraction Standards (JCPDS) database and literature data [32–36], as a reference. The XRD spectra of as-processed and oxidized samples are compared in Fig. 1, while the phases detected by XRD in the samples under investigation are compared in Table 1.

3.1.1. Oxidation of uncoated alloys

Before oxidation in burner rig apparatus, the XRD patterns of uncoated alloys show the peaks belonging to γ-TiAl and α_2-Ti_3Al crystalline phases (Fig. 1 a, c, e). The γ-TiAl presents ordered face-centred tetragonal $L1_0$ structure and α_2-Ti_3Al has ordered hexagonal $D0_{19}$ structure (refers to JCPDS No. 00-065-0428 and 00-052-0859 respectively). In the XRD patterns of TNM and HNb alloys also a peak at 2θ = 40.25° can be observed. This signal can be attributed to the (1 1 0) diffraction peak of cubic β-TiAl, whose formation is promoted by the rather high concentration of Nb and Mo in these alloys [37]. In every case, the relative intensities of the diffraction peaks of these phases show that γ-TiAl is the main component of the microstructure.

After 100 or 200 cycles under oxidizing atmosphere in the burner rig apparatus the XRD patterns of all the uncoated alloys were very similar, and showed the formation of titanium and aluminium oxides (Fig. 1 a, c, e). The (1 1 0) and (2 1 1) reflexes, which are the most important peaks of rutile with relative intensity of 100 and 60 respectively, can be clearly distinguished at 2θ = 27.5° and 2θ = 54.3° (refers to JCPDS No. 00-021-1276). Other diffraction peaks of rutile are superimposed to those characteristics of the phases pre-

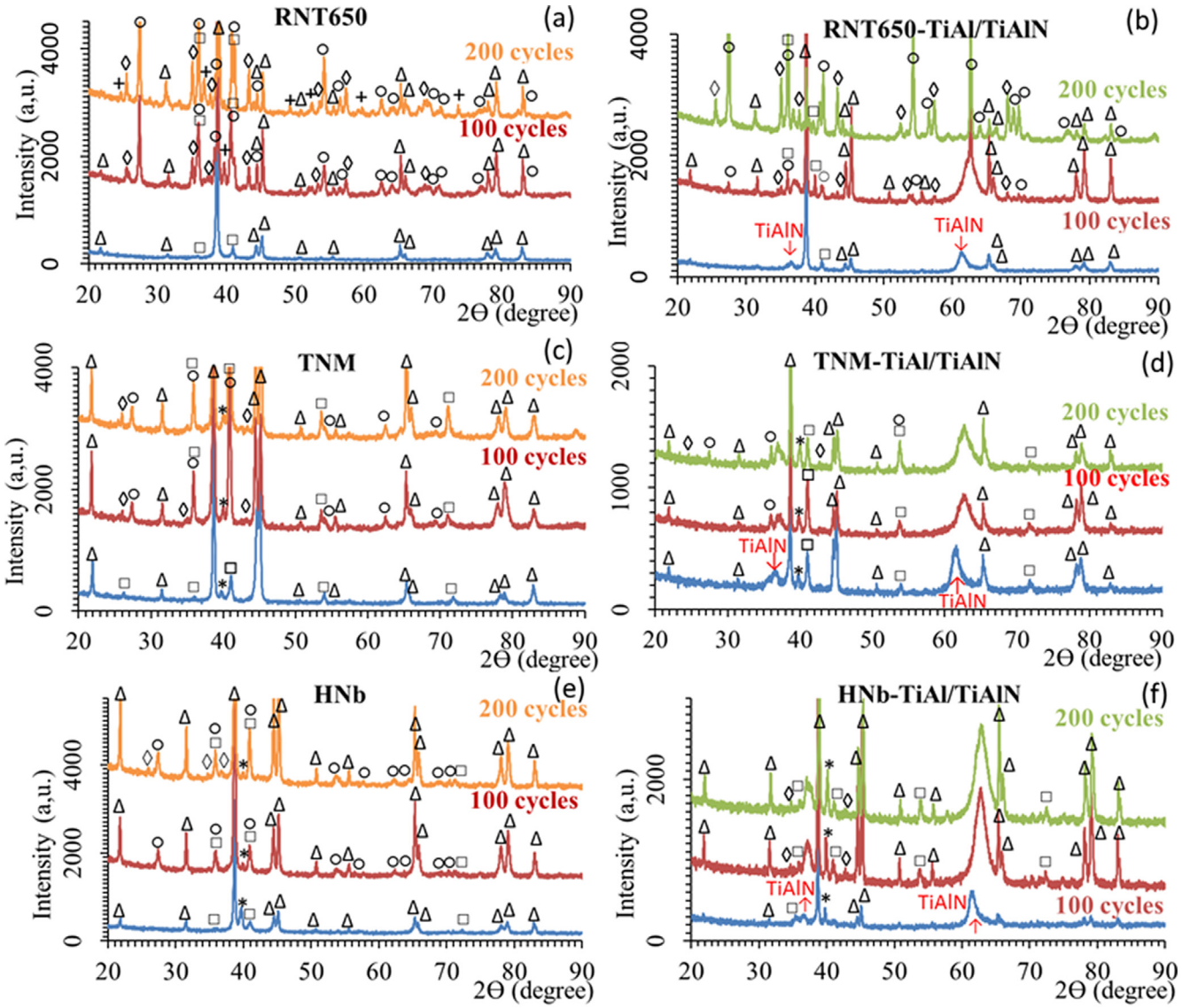

Fig. 1. XRD of as-processed samples and samples after oxidation (100 and 200 cycles) in burner rig apparatus at 1000 °C: a) uncoated RNT, b) coated RNT, c) uncoated TNM, d) coated TNM, e) uncoated HNb, f) coated HNb. Where: △ = γ-TiAl, □ = α_2-Ti_3Al, * = β-TiAl, ○ = TiO_2, ◇ = Al_2O_3 and + = Impurity from burner rig facility.

Table 1
Phases detected by XRD analysis.

N° of cycles	Uncoated RNT	Coated RNT	Uncoated TNM	Coated TNM	Uncoated HNb	Coated HNb
0	γ-TiAl α_2-Ti_3Al	γ-TiAl α_2-Ti_3Al TiAlN	γ-TiAl α_2-Ti_3Al β-TiAl	γ-TiAl α_2-Ti_3Al β-TiAl TiAlN	γ-TiAl α_2-Ti_3Al β-TiAl	γ-TiAl α_2-Ti_3Al β-TiAl TiAlN
100	γ-TiAl α_2-Ti_3Al TiO_2 Al_2O_3	γ-TiAl α_2-Ti_3Al TiAlN TiO_2 (Al_2O_3)*	γ-TiAl α_2-Ti_3Al β-TiAl TiO_2 (Al_2O_3)*	γ-TiAl α_2-Ti_3Al β-TiAl TiAlN (TiO_2)*	γ-TiAl α_2-Ti_3Al β-TiAl TiO_2	γ-TiAl α_2-Ti_3Al β-TiAl TiAlN (Al_2O_3)*
200	γ-TiAl α_2-Ti_3Al TiO_2 Al_2O_3	γ-TiAl α_2-Ti_3Al TiO_2 Al_2O_3	γ-TiAl α_2-Ti_3Al β-TiAl TiO_2 Al_2O_3	γ-TiAl α_2-Ti_3Al β-TiAl TiAlN (TiO_2)* (Al_2O_3)*	γ-TiAl α_2-Ti_3Al β-TiAl TiO_2 (Al_2O_3)*	γ-TiAl α_2-Ti_3Al β-TiAl TiAlN (Al_2O_3)*

* Very weak intensity of diffraction peaks.

sent before oxidation that are still well visible. From this feature it can be inferred that the oxide scale formed during the burner rig test is too thin for shielding the substrate from X-rays. The XRD patterns after oxidation show that also aluminium oxide forms. The (0 1 2), (1 0 4) and (1 1 3) peaks of corundum can be identified at 2θ angles equal to 25.6°, 35.2° and 43.4° (refers to JCPDS No. 00-042-1468). Even though they are among the more intense peaks of this aluminium oxide (relative intensities 70, 97 and 100 respectively), their intensity was negligible with respect to that of rutile peaks, thus showing that rutile was in every case the main oxidation product. Other very weak diffraction peaks were sometimes detected after long-term oxidation; very likely they can be attributed to particles present in the burner rig environment that contaminated the sample surface.

3.1.2. Oxidation of coated alloys

The as-processed coated alloys exhibited two additional peaks (with respect to the uncoated ones) in their XRD patterns at 2θ = 36.65° and 2θ = 61.61° (Fig. 1 b, d, f). These signals can be assigned to (1 1 1) and (2 2 0) diffraction peaks of TiAlN, that forms when aluminium atoms partially substitute titanium in TiN lattice (B1 NaCl-type) [33,36,38]. The intensity of (2 2 0) diffraction peak was much higher than that of the (1 1 1) one (higher than expected on the base of their relative intensities in TiAl and AlN XRD patterns), which means that TiAlN shows texture. In fact, magnetron sputtering based technologies are known to cause sturdy coating texture. The orientation of films is intensively influenced by ion bombardment during the film growth; actually (2 2 0) texture was already reported in the literature for TiAlN coatings [35,36,38]. However different kinds of texture can be observed depending on the composition of the TiAlN solid solution and the processing parameters adopted for the coating deposition [34–36,38].

The position of (2 2 0) TiAlN peak is shifted towards lower angles with respect to the position of (2 2 0) peak in the XRD patterns of both cubic TiN and AlN. This shift can be related to the compression residual stresses that are caused by the thermal expansion mismatch between the coating and the alloy. Elastic stresses can reasonably arise during the cooling from 400 °C after the coating deposition. Compression stresses act in the direction parallel to the (2 2 0) planes, which in turn are stacked parallel to the surface owing to texture, thus causing an increase of the interspace between these planes and a decrease of the 2θ angle. A similar effect, but less marked, was also observed for the (1 1 1) diffraction peak.

The other diffraction peaks of the TiAlN lattice cannot be distinguished because they are overlapped with strong reflexes of TiAl and Ti_3Al, which can be seen also after oxidation. Actually, the TiAlN coating is very thin, and therefore the X-rays can pass through this film and reach the intermetallic substrate. As a consequence, the diffraction peaks of γ-TiAl, α_2-Ti_3Al and β-TiAl were always present in the X-ray diffractograms of coated samples. Thermal cycling in oxidizing environment caused oxidation of coated alloys, as shown by the growth of weak peaks belonging to rutile and alumina in the relevant XRD patterns (Fig. 1 b, d, f).

Moreover, the XRD patterns of the coated RNT after 100 and 200 oxidation cycles (Fig. 1 b) showed some differences with respect to the XRD patterns of coated TNM and HNb alloys submitted to the same cyclic oxidation treatment (Fig. 1 d, f). In fact, a sharp peak superimposed to the broad (2 2 0) reflex of TiAlN solid solution and placed at 2θ = 62.7° appeared after 100 cycles. This peak, that can be tentatively attributed to (0 0 2) reflex of TiO_2, became much stronger after 200 cycles, while at the same time the TiAlN (1 1 1) and (2 2 0) peaks disappeared. Also other peaks attributed to rutile and alumina grew with the number of cycles, but the intensities of reflexes belonging to rutile still remained stronger than those of alumina, thus showing that rutile was the main component of the oxide layer grown on the surface of coated RNT.

The coated TNM and HNb alloys behaved in a rather different manner with respect to the RNT one, since their XRD patterns were almost unchanged after the burner rig test (Fig. 1 d, f). The (1 1 1) and (2 2 0) peaks of TiAlN were still well evident after oxidation, even though the position of (2 2 0) peak slightly shifted towards higher angles. This shift could depend on the complex thermal history of the samples, possibly involving solid state diffusion and thermal stress relaxation. In fact, stress relaxation should occur during the stay at 1000 °C in burner rig and result in a shift of the (2 2 0) peak towards higher 2θ angles.

Contrary to what happened in the case of coated RNT, only very weak peaks of rutile and alumina could be detected after oxidation in the XRD patterns of coated TNM and HNb (Fig. 1 d, f). In the case of TNM the intensities of peaks attributed to TiO_2 and Al_2O_3 were very similar, while only weak signals due to Al_2O_3 formation were found in the XRD pattern of HNb.

Conclusively, all these findings demonstrate that the effectiveness of the nitride coating is affected by the intermetallic substrate. Prolonged oxidation at high temperature destroys the coating deposited on RNT alloy, while this protective coating performs much better when deposited on the surface of TNM or HNb alloys since it greatly limits the amount of formed oxides.

3.2. Morphology of coatings and growing oxide layers (SEM analysis)

The SEM images of the cross-section of the samples under investigation are compared in Fig. 2. The phases constituting external part of the samples (oxide layer, nitride coating and TiAl interlayer) were assessed by SEM-EDS analysis.

The borders between neighbour layers are put in evidence by straight lines to make easier the evaluation of the layer thicknesses and the layers are labelled depending on their different composition (M_xO_y identifies the oxide layer made of a mixture of oxides, while the protective coating and the interlayer are labelled as TiAlN and TiAl respectively).

3.2.1. Oxide layer grown on uncoated alloys

The progressive growth of the oxide layer with the increase of the number of cycles can be well appreciated for the uncoated intermetallic alloys. The oxide layers formed on TNM and HNb surface look as homogeneous and pore free, and show regular thickness and flat interface with the substrate (Fig. 2 b, c, e, f). On the contrary, the oxide scale grown on RNT shows irregular thickness, wavy interface with the substrate and seems constituted by two parts with different morphology (Fig. 2 a, d). This last feature is well evident after 100 oxidation cycles, since the inner part of the layer shows a columnar structure, differently from the outer part. However, the EDS analysis put in evidence a not homogeneous composition of each part of the oxide scale and some differences between them (Al:Ti ratio). After 100 and 200 cycles in burner rig the uncoated RNT, TNM and HNb alloys showed oxide scales with different thicknesses as summarized in Table 2a.

A layer with thickness lower than 1 μm formed after 100 cycles on the surface of the TNM and HNb alloys, while a structured scale with irregular thickness ranging between 3 μm and 4.9 μm covered the surface of RNT alloy. This is not surprising, since it was previously reported that the oxidation resistance of these alloys changes according to the presence of different alloying elements [10]. Anyway, the ranking of oxidation resistance was also confirmed by the burner rig test. These outcomes prove that only a proper combination of alloying elements (like Nb, Mo and Cr) can appreciably improve the oxidation of TiAl alloys. The thickness of all the oxide scales further increased up to 200 cycles, but with different growing rates for the three TiAl intermetallic alloys under investigation.

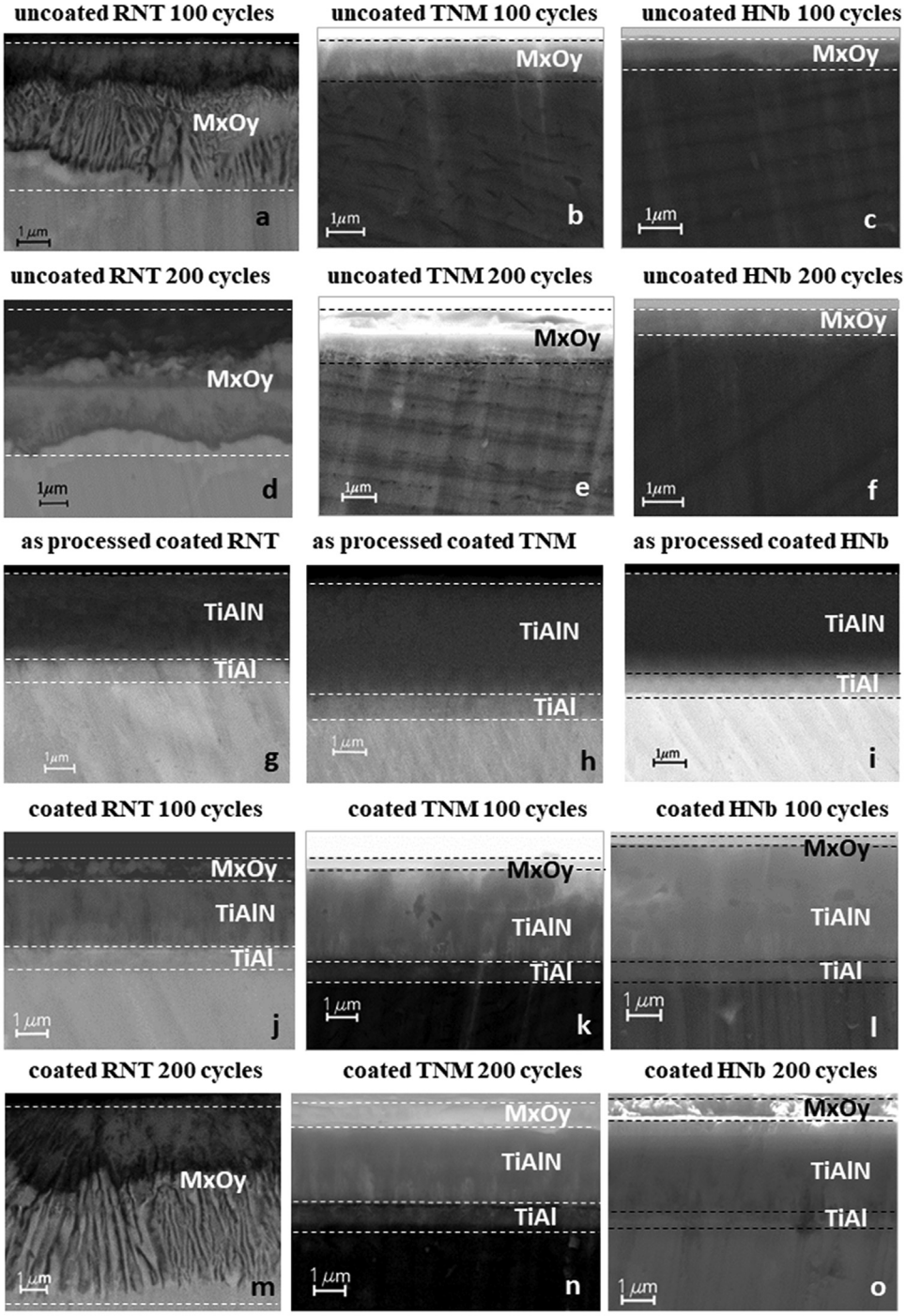

Fig. 2. SEM cross-section imagines of uncoated (a-f) and coated alloys (g-o) before and after oxidation at 1000 °C in burner rig apparatus. The borders between layers with different composition are put in evidence by straight lines. The composition of each layer is labelled as: M_xO_y = oxidized layer containing several oxides (namely Al_2O_3, TiO_2 and TiO_x), TiAlN = protective coating, TiAl = interlayer put in between the coating and the intermetallic substrate.

The final oxide scale was less than 1 μm thick or less than 2 μm thick for HNb and TNM respectively, while its thickness ranged between 4 μm and 6 μm for RNT (Fig. 2 d, e, f). However, it was hard to measure accurately the thickness of the oxide formed on RNT surface because spallation was also observed.

The RNT alloy, which currently should operate in service at temperatures below 800–850 °C [10], showed lower oxidation resistance than TNM and HNb alloys, that are designed for granting enhanced mechanical features and oxidation behaviour at higher temperatures.

3.2.2. Oxide layer grown on coated alloys

The TiAl interlayer and the outer TiAlN coating can be clearly seen in the cross section of all the as-processed coated alloys (Fig. 2 g, h, i). The thicknesses of all these TiAlN coatings was about 3.6 μm and that of TiAl interlayer was about 0.5 μm. Therefore, the magnetron sputtering process adopted for the film deposition gave the same results, irrespectively from the composition of the TiAl substrate. The formation of the oxide layer on these coated samples during the burner rig test is depicted in Fig. 2. The thickness of the TiAlN coating and the TiAl interlayer before

Table 2
a. Thicknesses of oxides layers grown on uncoated samples (SEM-EDS).

Uncoated Alloys	Treatment conditions		
	As-processed	100 cycles at 1000 °C	200 cycles at 1000 °C
RNT	–	oxide (ext.) 1–2 μm oxide (int.) 2–2.9 μm	oxide (ext.) 2–3 μm oxide (int.) 2–3 μm
TNM	–	oxide ~ 1 μm	oxide ~ 1.5 μm
HNb	–	oxide ~ 0.5 μm	oxide ~ 0.9 μm

b. Thicknesses of growing oxides layers and change of coatings thickness due to oxidation (SEM-EDS).

Coated Alloys	As-processed	100 cycles at 1000°C	200 cycles at 1000°C
RNT coated	TiAl ~ 0.5μm TiAlN ~ 3.6μm	TiAl ~ 0.5μm TiAlN ~ 2.1μm oxide ~ 0.7μm	oxide (ext.) ~ 2.2μm oxide (int.) ≤ 4.3μm
TNM coated	TiAl ~ 0.5μm TiAlN ~ 3.6μm	TiAl ~ 0.5μm TiAlN ~ 3.2μm oxide ~ 0.4μm	TiAl ~ 0.5μm TiAlN ~ 2.5μm oxide ~ 0.7μm
HNb coated	TiAl ~ 0.5μm TiAlN ~ 3.6μm	TiAl ~ 0.5μm TiAlN ~ 3.4μm oxide ~ 0.2μm	TiAl ~ 0.5μm TiAlN ~ 3.2μm oxide ~ 0.7μm

and after testing, as well as the thickness of the oxide scale, are reported in Table 2b.

A regular and homogeneous oxide layer slowly grew on TNM-TiAl/TiAlN and HNb-TiAl/TiAlN samples after 100 or 200 cycles in the burner rig apparatus (Fig. 2 k, l, n,o). A similar oxide layer with just a bit greater thickness was also observed after 100 cycles on the surface of RNT-TiAl/TiAlN sample (Fig. 2 j). In every case, the morphology of the underlying protective coating was unchanged after oxidation.

Table 2b shows that after short-term oxidation (100 cycles), the TiAlN coatings appeared only slightly oxidized, since oxide scales always less than 1 μm thick grew on every coated alloy. However, the oxide layer grown on coated RNT (0.7 μm thick) was two or three times thicker than that observed on TNM or HNb (0.4 μm and 0.2 μm respectively). Also the TiAlN coatings were differently consumed by oxidation depending on the various substrates that they covered, in fact after 100 cycles the coating thicknesses decreased of 0.2 μm, 0.4 μm and 1.5 μm respectively when deposited on HNb, TNM and RTN alloys. On the contrary the TiAl interlayer kept its morphology and thickness unchanged during this test. This first oxidation test (100 cycles) did not put in evidence very important differences in the oxidation behaviour of the different materials, which means that during the initial oxidation the nitride coating performs in the same manner irrespectively from the underlying substrate.

On the contrary, the oxidation response of the materials under investigation appreciably differed when the burner rig test was prolonged to 200 cycles. In this case the thickness of the oxide layer grew up to 0.7 μm on the TiAlN coating deposited on HNb substrate, while in the meantime the thickness of the coating decreased from 3.6 to 3.2 μm. The behaviour of the coated TNM was only a bit worse, since the thickness of the scale increased up to about 0.7 μm and that of the coating reduced to 2.5 μm. On the contrary, the burner rig test repeated for 200 cycles had a dramatic effect on the coated RNT.

Actually, the TiAlN coating and TiAl interlayer deposited on RNT alloy were completely consumed, and replaced by a very thick scale showing a complex microstructure (Fig. 2 m). This oxide scale was made by two parts: an external one about 2.2 μm thick and an internal one with columnar structure and thickness of about 4.3 μm. It should be noticed that the morphology of the scale is very similar to that observed after testing in burner rig (100 cycles) the uncoated RNT alloy (Fig. 2 a), which demonstrates as the prolonged thermal cycling in oxidizing environment destroys the protective coating deposited on RNT substrate and eliminates its beneficial effect.

3.3. XPS investigation of the composition of the oxide layer

The XPS investigation of the part of the oxide layer facing the oxidizing atmosphere was carried out after the test in burner rig apparatus (100 and 200 cycles) with the aim of strengthening the XRD outcomes, suggesting that the presence of a protective TiAlN coating can affect the kind of oxides constituting the oxide scale. Particular attention was also put at the detection of the alloying elements formerly present only inside the intermetallic substrate. In fact, their presence inside the oxide layer would prove that they can diffuse towards the oxide layer growing on the surface. It is well known that XPS analysis gives information about the composition and the relevant chemical bonds of species present in a very thin layer on the sample surface. For this reason, it is a powerful tool for assessing if a passive layer forms on the surface or not. The XPS survey was adopted in order to assess the general composition of the external part of the oxide layer, looking for the ratio between elements that can give rise to passive layers and other elements forming oxides. Some weak signals found in the survey XPS spectra can be attributed to the contamination of the sample surface. Actually, the burner rig testing apparatus involves the use of a burner, sample holders and high temperatures that can cause this contamination. Carbon and nitrogen can come from the gaseous atmosphere in the burner rig apparatus, while elements coming from the sample holder (like Fe) are responsible for weak peaks and background noise sometimes observed in the region of binding energy between 600 and 900 eV. For this reason, all samples were gentle polished by argon sputtering before the XPS analyses. In spite of this polishing step some contamination still remained giving signals inside the XPS spectra. These signals attributable to surface contamination were not investigated and therefore are not discussed in the following. The results of XPS survey are summarized in Table 3.

High resolution spectra (HRS) of the main elements found inside the growing oxide layer were also recorded (Figs. 3-8); the fitting of these spectra was used to investigate possible formation of passive layers. Of course, elements contained in small quantity were not subjected to deep investigations by means of high resolution spectra. In these cases, the HSR of the element shows a very weak peak with very irregular shape, which makes very hard to perform a fitting.

Only the fitting of high resolution spectra of selected elements (forming to the most important components of the oxide scale) was carried out by using binding energies reported in the literature and adopted in previous investigations on TiAlN oxidation [20].

Table 3
XPS survey analysis of the surfaces of oxidised samples (100 and 200 cycles) after cleaning by argon sputtering.

Atomic, %	RNT	RNT 100 cycles	RNT 200 cycles	RNT coated 100 cycles	RNT coated 200 cycles
O	–	62.6	66.0	65.3	64.6
Ti	49	20.4	17.0	3.1	23.2
Al	48	13.2	12.8	25.1	11.3
Cr	0.7	3.0	1.5	1.8	0.4
Nb	2	0.1	0.1	0.1	0.1
Si	0.3	0.7	2.6	4.6	0.4
	TNM	**TNM 100 cycles**	**TNM 200 cycles**	**TNM coated 100 cycles**	**TNM coated 200 cycles**
O	–	65.1	67.8	62.6	67.0
Ti	51.5	15.1	19.6	2.5	1.2
Al	43.5	19.5	12.4	34.7	31.6
Nb	4	0.2	0.1	0.1	0.1
Mo	1	0.1	0.1	0.1	0.1
	HNb	**HNb 100 cycles**	**HNb 200 cycles**	**HNb coated 100 cycles**	**HNb coated 200 cycles**
O	–	63.4	69.5	63.5	63.5
Ti	43	17.2	13.3	1.4	1.2
Al	47	15.4	13.6	30.8	30.0
Cr	2	3.9	3.3	4.2	5.1
Nb	8	0.1	0.3	0.1	0.2

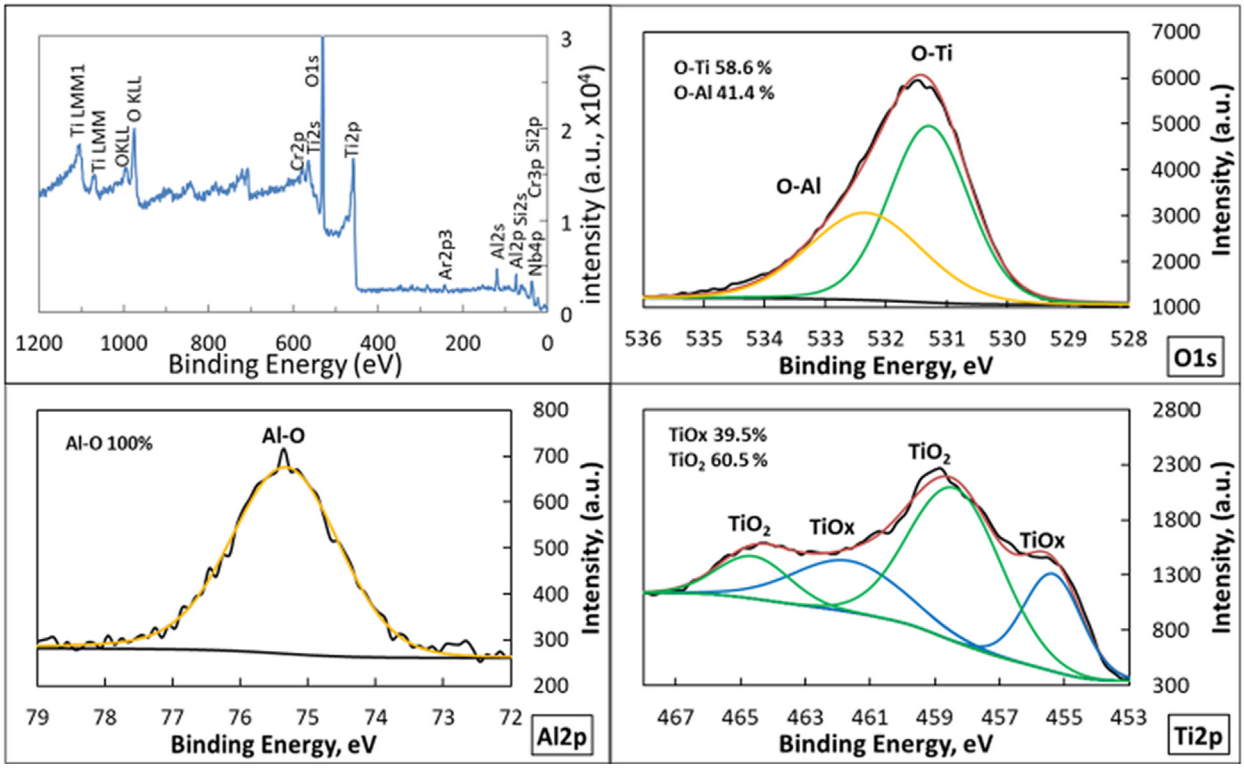

Fig. 3. XPS analysis of oxidized surface of uncoated RNT after 100 cycles at 1000° in burner rig apparatus (black curve = experimental signal, red curve = sum of the fitting components, yellow curve = aluminium oxide, green and blue curves = titanium oxides). (For interpretation of the references to colour in this figure legend, the reader is referred to the web version of this article.)

3.3.1. XPS investigation of uncoated and coated RNT alloy

The XPS survey and the high resolution spectra of uncoated and coated RNT alloy after 100 cycles of treatment in burner rig are reported in Fig. 3 and Fig. 4 respectively, while the surface chemical composition after 100 and 200 cycles of treatment are compared in Table 3.

After oxidation at 1000 °C the presence of O, Ti, Al, Cr, Nb and Si was detected by XPS on the surface of both uncoated and coated RNT alloy. Very weak signals attributable to surface contamination were also found in the range between 700 and 900 eV.

The XPS quantitative chemical analysis of the sample surface after oxidation showed that Ti, Al and O were the main components of the oxide layer (Table 3), but very different Al:Ti ratio could be observed. Titanium and aluminium were present in similar amounts on the surface of uncoated RNT after 100 or 200 cycles of oxidation, while mostly aluminium and oxygen (forming alumina) were detected in the outer part of the scale formed on coated RNT after 100 cycles. In this case, concentrations of 25.1% at. and 3.1% at. were here measured for Al and Ti respectively (Table 3). The relative amount of these elements measured by XPS greatly

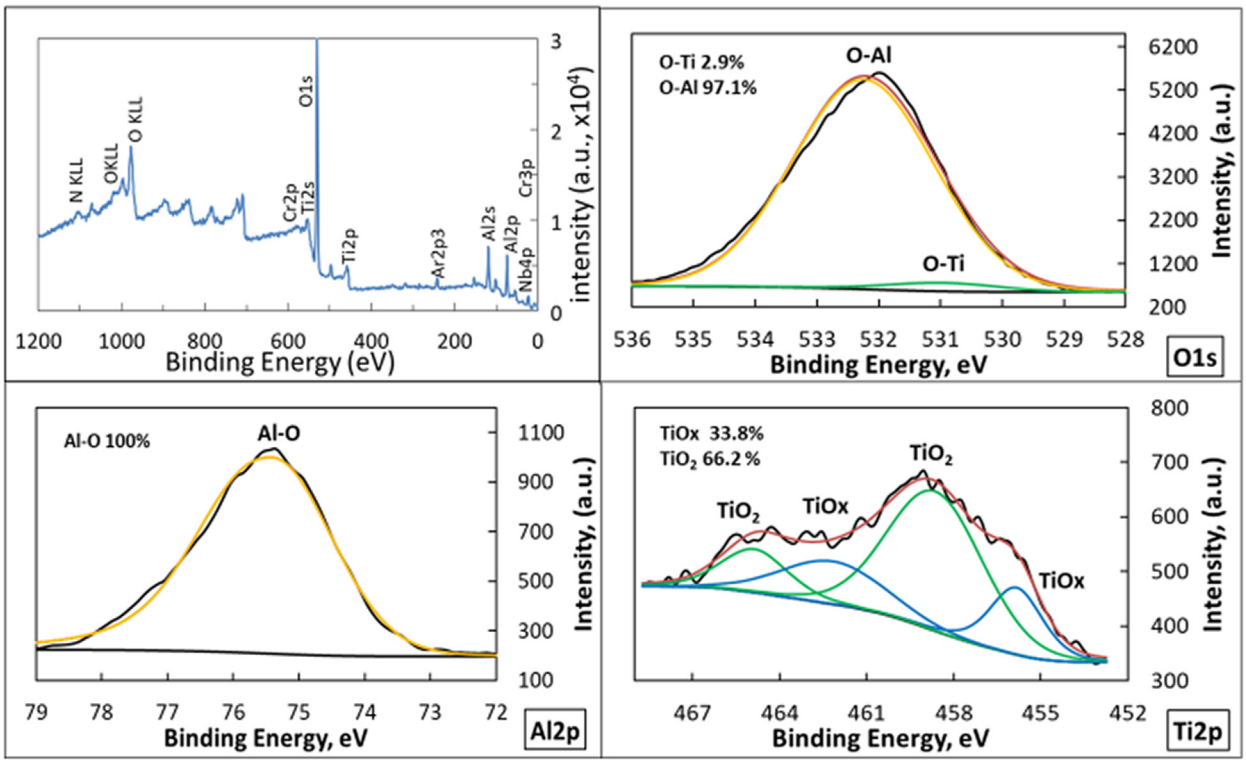

Fig. 4. XPS analysis of oxidized surface of coated RNT after 100 cycles at 1000° in burner rig apparatus (black curve = experimental signal, red curve = sum of the fitting components, yellow curve = aluminium oxide, green and blue curves = titanium oxides). (For interpretation of the references to colour in this figure legend, the reader is referred to the web version of this article.)

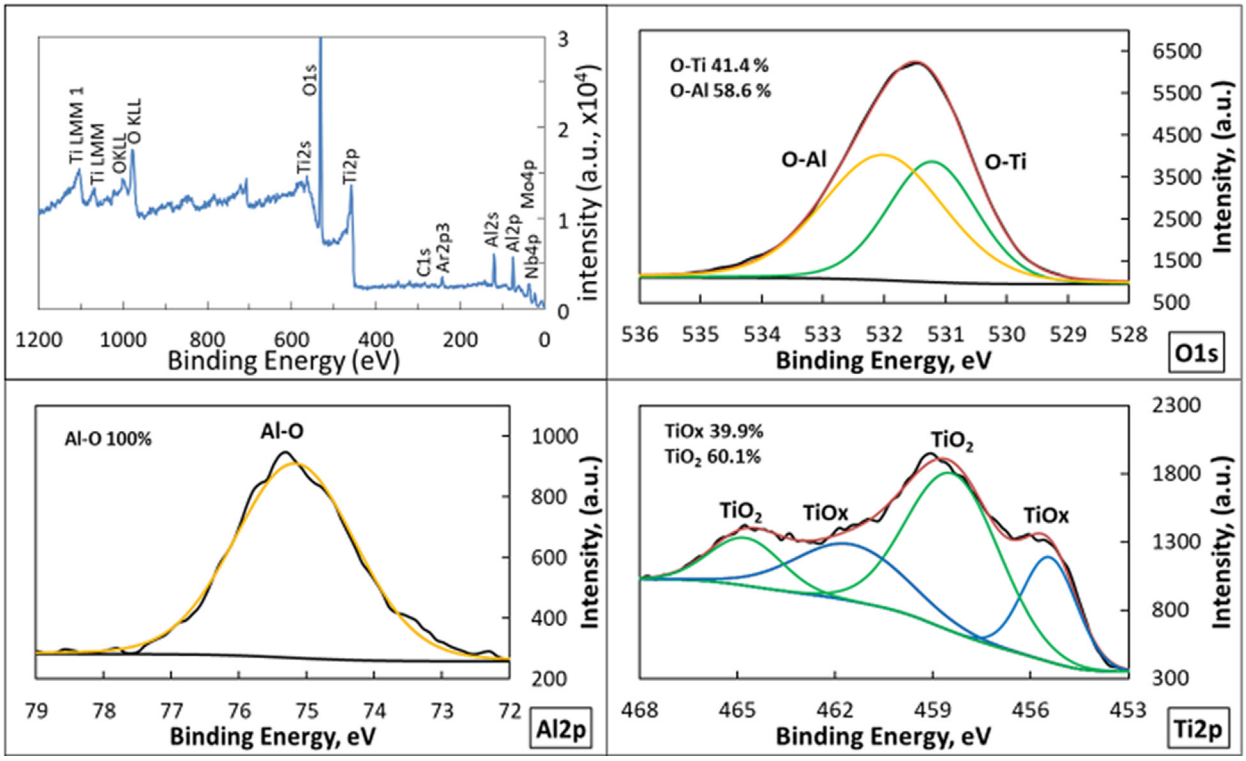

Fig. 5. XPS analysis of oxidized surface of uncoated TNM after 100 cycles at 1000° in burner rig apparatus (black curve = experimental signal, red curve = sum of the fitting components, yellow curve = aluminium oxide, green and blue curves = titanium oxides). (For interpretation of the references to colour in this figure legend, the reader is referred to the web version of this article.)

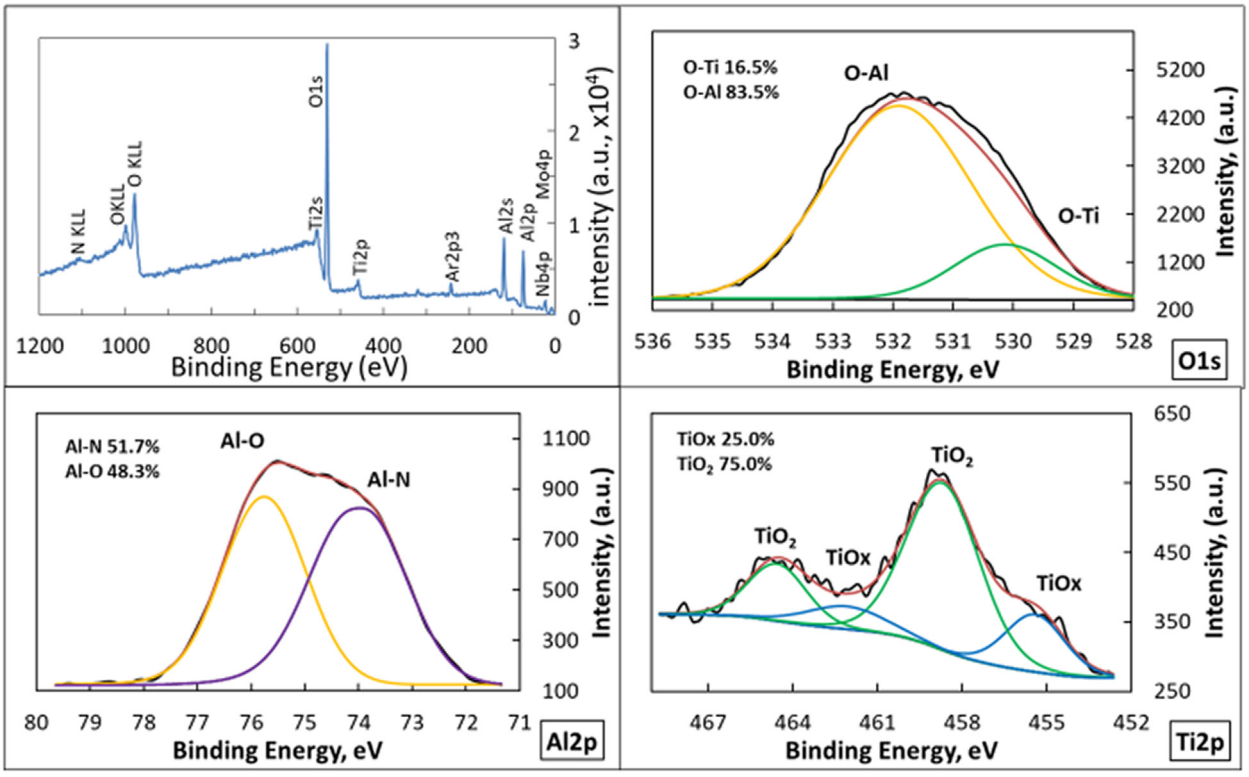

Fig. 6. XPS analysis of oxidized surface of coated TNM after 100 cycles at 1000° in burner rig apparatus (black curve = experimental signal, red curve = sum of the fitting components, yellow curve = aluminium oxide, green and blue curves = titanium oxides). (For interpretation of the references to colour in this figure legend, the reader is referred to the web version of this article.)

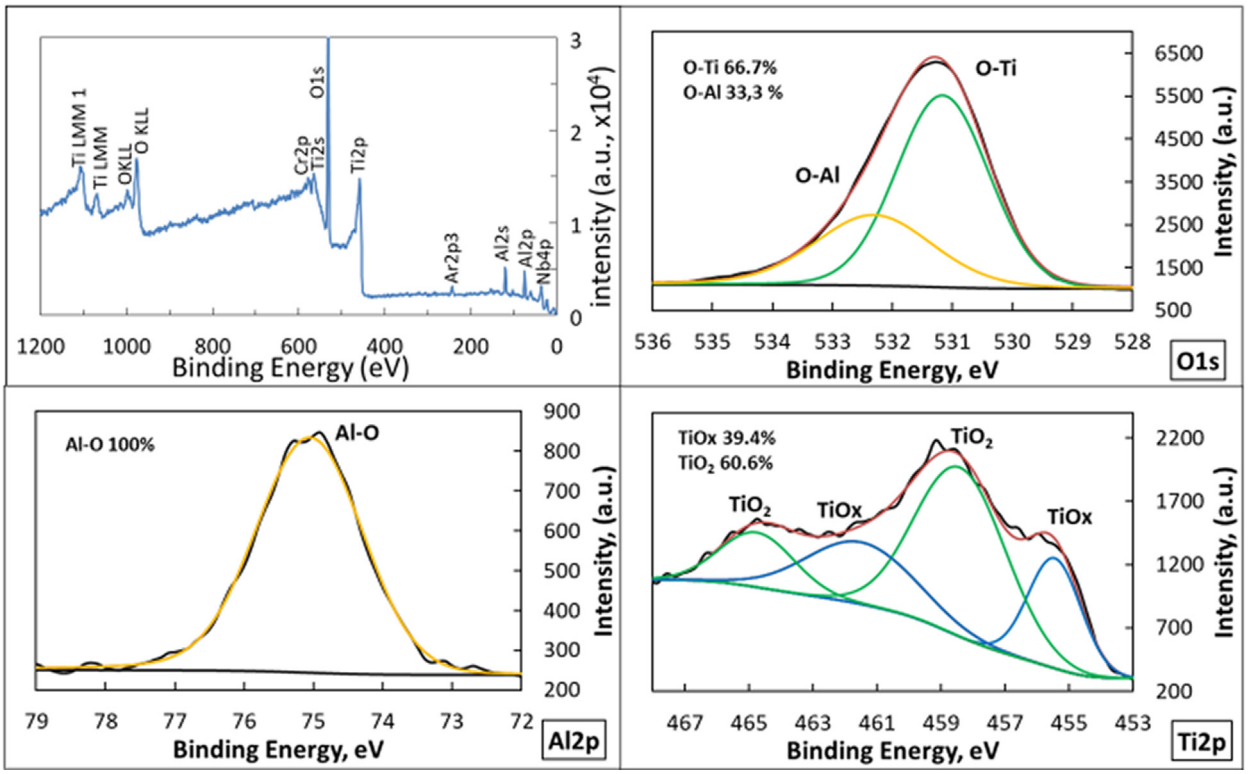

Fig. 7. XPS analysis of oxidized surface of uncoated HNb after 100 cycles at 1000° in burner rig apparatus (black curve = experimental signal, red curve = sum of the fitting components, yellow curve = aluminium oxide, green and blue curves = titanium oxides). (For interpretation of the references to colour in this figure legend, the reader is referred to the web version of this article.)

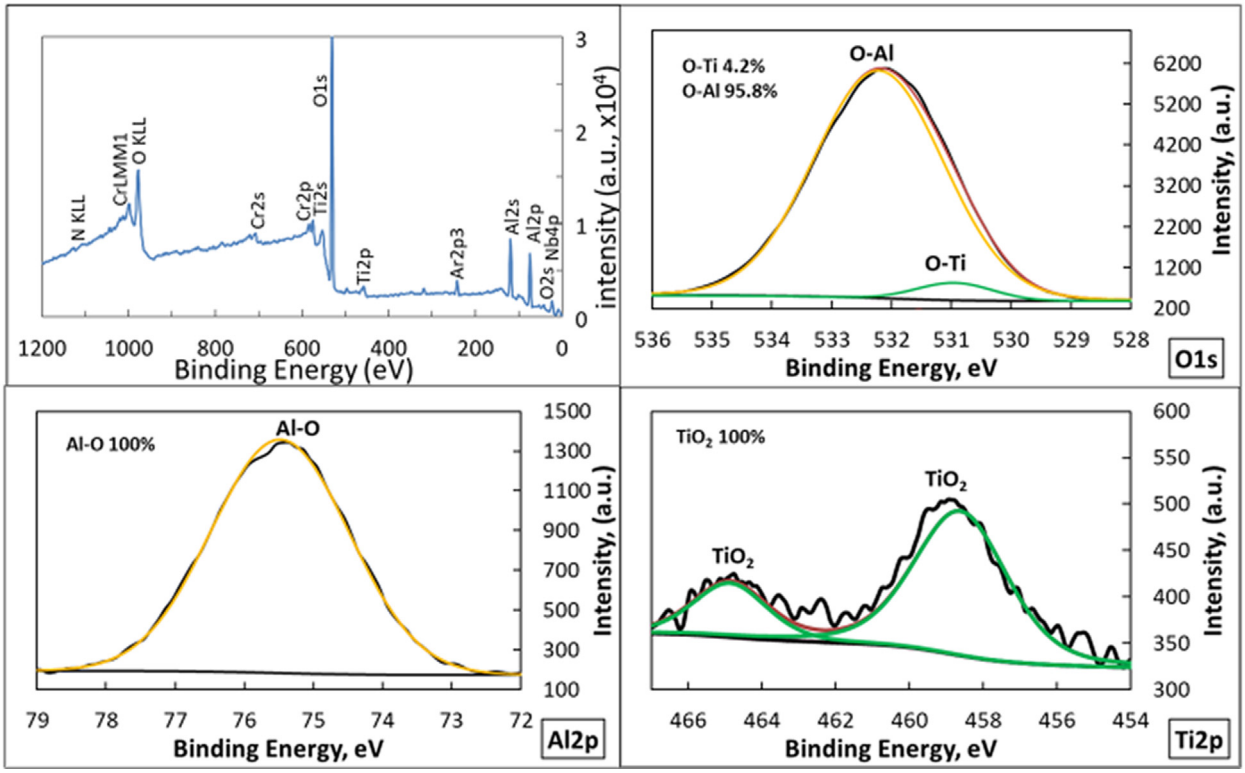

Fig. 8. XPS analysis of oxidized surface of coated HNb after 100 cycles at 1000° in burner rig apparatus (black curve = experimental signal, red curve = sum of the fitting components, yellow curve = aluminium oxide, green and blue curves = titanium oxides). (For interpretation of the references to colour in this figure legend, the reader is referred to the web version of this article.)

changed after 200 cycles because the concentrations of Al and Ti became 11.3% and 23.2% respectively (Table 3). Conclusively, XPS investigations proved that, at the end of 200 cycles, the oxide layer was made of a mixture of TiO2 and Al2O3, as in the case of the scale grown on the alloy not protected by the coating. On the other hand, after 200 cycles the TiAlN coating was completely consumed by oxidation (as showed by SEM and XRD investigations), and then it was not able to affect any longer the ratio between Al2O3 and TiO2 in the eternal part of the oxide scale. Important concentrations of silicon and chromium (much higher than in the substrate) were detected in the scale grown on uncoated RNT after 100 and 200 cycles, as well as in the layer formed on the coated alloy after 100 cycles. In this last case (coated RNT), this outcome proved that solid state diffusion of Cr and Si through the TiAlN coating occurred. On the contrary, only traces of Nb were always found in the oxide scale.

The high resolution spectra also highlighted the different response between uncoated and coated RNT (Figs. 3 and 4). In every case the O1s spectra put in evidence the formation of titanium and aluminium oxides, but with very different proportions. In fact, these high resolution spectra can be fitted by two peaks which are characteristic of O-Al and O-Ti bonds. According to the literature, as discussed in a previous paper [20], the binding energy for the O-Al bond is placed at 532.1 eV while literature reports values of binding energy for O-Ti bond that ranges between 529.6 eV and 531.2 eV. The integration of the peaks representing these two components shows that the amount of titanium oxide is well over that of the aluminium oxide within the oxide layer grown on the uncoated alloy (Fig. 3), while the surface of the scale formed on the coated alloy is almost completely constituted by aluminium oxide (Fig. 4). The Ti2p high-resolution spectra (HRS) showed a complex and irregular structure, in particular when recorded on the oxidized surface of coated RNT that contains about 3% at. of Ti only (Fig. 3). Even though the irregular profile of Ti2p HRS makes difficult their deconvolution, they prove the formation of two titanium oxides: TiO_2 and TiO_x, which is a non-stoichiometric oxide with composition ranging between $TiO_{0.7}$ and $TiO_{1.3}$ [39]. Anyway, according to the peak deconvolution of the HR Ti2p spectrum the main component of the mixture of titanium oxides was TiO_2.

The Ti2p high-resolution spectra (Figs. 3 and 4) put in evidence two different spin orbit doublets. According to the literature, the TiO_2 doublet is placed at 458.3–458.7 eV ($Ti2p_{3/2}$) and 464.3–463.5 eV ($Ti2p_{1/2}$) [34,40], while the TiO_x doublet is placed at 455.3–456.2 eV ($Ti2p_{3/2}$) and 461.7–462.8 eV ($Ti2p_{1/2}$) [20]. Finally, the high resolution spectra of Al2p showed exclusively the peak of Al-O bond with binding energy of 75.6 eV, which is characteristic of alumina [20].

3.3.2. XPS investigation of uncoated and coated TNM alloy

The XPS survey analysis showed that the oxide layer formed on uncoated TNM contained similar amounts of titanium and aluminium while the outermost part of the scale grown on the protective coating contained almost exclusively alumina (Table 3). This observation confirms that the TiAlN coating, as previously discussed for RNT alloy, favours the formation of alumina in the external part of the oxide layer. Only negligible amounts of Mo and Nb were always observed within the oxide scale obtained on both uncoated and coated TNM samples. This means that these alloying elements (that make the 5% at. of the substrate) hardly can diffuse from the intermetallic towards the surface and take part to the formation of the oxide layer.

The comparison between the high resolution XPS spectra of uncoated TNM (Fig. 5) and of coated TNM (Fig. 6) confirmed that the TiAlN coating greatly affected the oxidation process. The O_{1s} HR spectrum showed that oxygen was always bonded to Ti and Al, and then that the oxide scale was made of a mixture of the Ti

and Al oxides. Once again, the proportion between titanium oxide and aluminium oxide greatly depended on the presence of the coating. In fact, the content of these two oxides was similar when the coating was absent (Fig. 5), while the surface of the oxide layer was almost completely constituted by alumina when the sample was protected by the TiAlN coating (Fgure 6).

The Al2p HR spectrum showed a maximum that fits with the energy of Al-O bonds typical of alumina, but in the case of the coated TNM the Al2p peak was broadened, so that the contribution of other chemical bonds formed by alumina should be considered for the fitting. The contribution of Al-N bonds could be tentatively used to fit the Al2p spectrum for coated TNM (Fig. 6). The Ti2p spectrum allowed to state, on the base of the discussion already done in the previous paragraph, that titanium manly oxidised to TiO_2, and that this oxide was mixed with a smaller amount of TiO_x.

3.3.3. XPS investigation of uncoated and coated HNb alloy

Table 3 summarizes the composition of the oxidized surface of uncoated and coated HNb samples. Fig. 7 and Fig. 8 depict the survey and the high resolution spectra recorded after oxidation. The survey of these samples put in evidence the presence of O, Ti, Al, Cr and Nb in the outermost part of the oxide scale.

The XPS quantitative analysis of the elements present on the surface of oxidized samples (Table 3) allows to state that the oxide scale formed on uncoated HNb is constituted by a mixture of titanium and aluminium oxides, while the external part of the scale formed on the coated alloy mainly consists of aluminium oxide. It is worth of notice that also chromium took part in the oxide scale formation. In fact, its concentration in the external part of the oxide layer was well over its content in the alloy, in particular in the case of samples carrying the TiAlN coating. On the contrary, only traces of Nb were found in the oxide scale, as happened for TNM and RNT alloys as well.

Also the O1s HR spectra of coated and uncoated samples demonstrated that the oxide layer chiefly contained titanium and aluminium oxides, but oxygen was almost completely bond to aluminium in the scale formed on the coated HNb.

Spectra of Al2p and Ti2p recorded on both uncoated and coated HNb confirmed that aluminium reacted with oxygen to give alumina (Figs. 7 and 8) while the titanium oxidation gave rise to a mixture of TiO_2 and TiO_x (Fig. 7), as also happened for the other alloys investigated, or resulted in the formation of TiO_2 only when the coated alloy suffered oxidation (Fig. 8).

3.3.4. Final remarks about XPS results

Summarizing, the XPS results confirmed that the oxidation of uncoated TiAl alloys with different compositions results in the formation of oxide scales with similar compositions, as the external part of the oxide layer was always constituted by a mixture TiO_2, Al_2O_3 and TiO_x.

Moreover, the amounts of aluminium and titanium oxides in the external part of the oxide layer was similar, as it was very similar the concentration of Ti and Al in the three alloys submitted to oxidation test in the burner rig apparatus. This result does not match well with the XRD outcomes, that showed as TiO_2 forms preferentially with respect to alumina. On the other hand, XRD analysis refers to the whole oxide layer while XPS analysis regards the external part of the oxide layer only. On the other hand, these three intermetallic alloys are believed to display different oxidation behaviour owing to the presence of different alloying elements (namely Cr, Si, Nb and Mo). Some beneficial effect could be attributed to silicon and chromium, since their concentration in the external part of the oxide scale was well over the content of these elements inside the substrate. On the contrary, only little contents of molybdenum and niobium, well below their concentration in the substrate, were detected on the surface of the oxide scale. All these findings bring to the conclusion that silicon and chromium quickly diffuse through the oxide scale and concentrate in its outer part, while niobium and molybdenum can hardly diffuse through the growing oxide scale. Nonetheless, Nb and Mo are believed to enhance the oxidation resistance of TiAl alloys, because their presence in the substrate decreases the solubility of oxygen in the intermetallic alloy [41–43].

The deposition of a TiAl/TiAlN protective coating had not any appreciable effect on the presence of alloying elements inside the oxide layer. In fact, molybdenum and niobium still did not take significant part in the scale formation while silicon and chromium were well present inside the oxide layer. This means that silicon and chromium can easily pass through the TiAlN coating, while the diffusion of Mo and Nb through the coating is difficult.

Moreover, the TiAlN coating deposited on the surface of these alloys greatly changed the composition of the growing oxide layer. In particular, the nitride coating was able to promote the formation of alumina in the external part of the scale. Actually, the ratio between Al and Ti was about 31:1.4 or 35:2.5 or 25:3 in the oxide layers formed on coated HNb, TNM and RNT samples respectively after 100 cycles (Table 3). On the other hand, both electron microscopy and X-ray diffraction showed that the effectiveness of the nitride protection coating depended also on the kind of intermetallic substrate on which it was deposited. Therefore, it should be inferred that different alloying elements also exert some influence on the oxidation behaviour of alloys carrying the same TiAlN-TiAl protective coating.

3.4. Chemical characterization of TiAlN coatings by SEM-EDS

As previously discussed, the kind of intermetallic substrate was found to affect either the effectiveness of the TiAlN protective coating or the composition of the oxide scale.

In principle, the presence of different alloying elements in the alloys under investigation could exert some influence on the thermal expansion mismatch between coating and substrate, but such an effect was not found, as coating spallation or cracking were never observed in this investigation. Therefore, it seemed sensible to investigate by SEM-EDS the effect of solid state diffusion on the change of composition of the nitride coatings, possibly occurring during the oxidation test. The SEM-EDS results are summarized in Table 4.

In the present work we assessed by SEM-EDS that the as processed TiAlN coatings showed 53–55% at. of nitrogen and an Al:Ti ratio close to 1:1. The content of nitrogen exceeding 50% at. suggests that cationic vacancies are present in these surface coatings. The presence of these cationic vacancies obviously can promote the diffusion of metallic elements through the nitride coating. The off-stoichimetry in TiAlN films, involving metal and nitrogen vacancies, was previously reported in the literature[44,45].

According to Baben et al. [44], that investigated the stoichiometry of $(TiAl)N_x$ metastable coatings processed by magnetron sputtering, the final stoichiometry of these coatings depends on the processing conditions in the magnetron sputtering equipment. In particular, a high concentration of nitrogen vacancies gives rise to values of x lower than one, while $x > 1$ can result from metal vacancies. Other authors too [46,47] observed off-stoichiometry of nitrogen in several TiAlN, TiAlCrN and TiAlSiN films deposited by unbalanced magnetron sputtering. In the present investigation off-stoichiometry of nitrogen was also observed after oxidation treatments, which caused a further increase of nitrogen concentration in TiAlN up to 59% at. (Table 4). Then a nitrogen enrichment occurred during the burner rig testing. This outcome agrees with literature, reporting that the TiAlN films hinder the inward diffusion of oxygen but not that of nitrogen, which can easily move towards the substrate [20].

Table 4
SEM-EDS analysis of the middle zone of TiAlN coatings after oxidation treatments. In case of RNT coated samples after 200 cycles the coating was replaced by a thick oxide layer showing two distinguished zones (internal and external), with different morphologies and composition as reported in the table.

Coated alloys	Composition, (% at.)						
	O	Ti	Al	Cr	Nb	Si	N
RNT coated 100 cycles	7.8	15.6	17.8	–	–	detected (<0.1)	58.8
RNT coated 200 cycles (ext.)	66.7	18.3	14.4	0.2	0.2	0.2	–
RNT coated 200 cycles (int.)	50.0	23.9	24.6	0.4	0.9	0.3	–
TNM coated 100 cycles	3.2	17.9	19.7	–	–	–	59.1
TNM coated 200 cycles	6.6	22.7	21.5	–	detected (<0.1)	–	49.2
HNb coated 100 cycles	4.0	19.4	21.0	–	–	–	55.6
HNb coated 200 cycles	6.0	17.3	20.2	–	–	–	56.5

However, oxidation tests also caused the diffusion of oxygen inside the coating, that resulted in oxygen percentages within the TiAlN ranging between about 3% at. and about 8% at., and depending on the number of cycles and the alloy carrying the protective film. The oxygen percentage increased with the number of cycles within the coatings placed on HNb and TNM. Moreover, the maximum oxygen content (about 8% at.) was observed already after 100 cycles in the TiAlN coating placed on the RNT substrate. This higher oxygen concentration suggests that the TiAlN-RNT sample is more prone to suffer oxidation. Conclusively, the composition of the TiAlN coating changed during the oxidation tests, in particular the content of oxygen progressively increased due to its diffusion through the oxide scale (Table 4). Table 4 also shows that the Al:Ti ratio inside the TiAlN coatings did not change appreciably with the progress of oxidation. However, it should be noticed that in the oxidized samples the content of Al was frequently higher than that of Ti (this is the case of the film placed on RNT and HNb substrates), while a ratio between these elements close to 1:1 was detected in the as processed coatings.

Dealing with the other metallic elements, the EDS results in Table 4 show that the concentrations of Nb, and Si inside the TiAlN coating were very low, while Mo (not reported in Table 4) and Cr were never detected by EDS. As a matter of fact, traces of Si and Nb were found in the nitride coating placed on RNT (after 100 cycles) and TNM (after 200 cycles) respectively. These results should be compared with the outcomes of XPS investigations carried out on the oxide scale (Table 3). In agreement with EDS results, XPS proved that only negligible amount of Mo and Nb can reach the oxide layer after diffusion through the TiAlN coating. On the contrary, XPS showed that after 100 cycles the concentrations of Si and Cr in the oxide scale grown on TiAlN-RNT system were respectively fifteen times and two times higher than inside the intermetallic substrate. Also the oxide layer formed on the TiAlN-HNb system contained more Cr than the underlying HNb alloy. The XPS and EDS outcomes proved that the diffusion of Cr and Si quickly occurred through the TiAlN coating, even though their concentrations inside the TiAlN layer still remained very low, as in the meantime they progressively accumulated within the oxide layer. The diffusion of Cr seems not to have any detrimental effect on the TiAlN oxidation resistance, since the TiAlN-HNb system (containing Cr) performed very well. As a consequence, the rather poor performance of the TiAlN-RNT system (containing both Cr and Si) should be ascribed only to silicon diffusion inside the coating.

According to the literature silicon shows a rather good solubility in TiAlN [48]. In addition, the presence of silicon in the TiAlN lattice strongly makes this solid solution not stable and locally promotes the formation of zones with different Al:Ti ratios; this effect was observed also when the Si concentration was very low [49,50]. Therefore, it can be inferred that the lack of TiAlN stability due to Si can result in the local formation of zones with a reduced aluminium content, which worsens the oxidation resistance of the coating. In fact, according to Saringer et al. [51] the oxidation resistance of Ti-Al-N phases increases with their Al content, irrespectively from their different crystalline structures, according to the following ranking: TiN < Ti0.5Al0.5 N < Ti0.1Al0.9 N < w-AlN.

4. Conclusions

Identical protective coatings made of an inner TiAl film and a thicker external TiAlN layer were deposited by HiPIMS on the surface of three TiAl intermetallics, and tested for the oxidation protection of these alloys at high temperature (up to 1000 °C). Uncoated alloys and coated samples were contemporaneously tested in a facility designed for simulating the oxidant environment and temperatures experienced by components of turbine engines. The effect of severe thermal cycling on the oxidation behaviour was also investigated. In spite of these severe experimental conditions the coatings proved to be very effective and well compatible with the metallic substrates, since coating cracking or debonding at the coating/substrate interfaces were never observed. The TiAl/TiAlN protection system greatly slowed down the oxidation of all the alloys investigated. Its effect was due to the formation of a passive alumina layer in the external part of the oxide scale. However, its effectiveness was found to depend also on the intermetallic alloy used as substrate. The best results were obtained when the coating was deposited on Ti-47Al- 2Cr-8Nb alloy and rather good effectiveness was observed also for the protection of Ti-43.5Al-4Nb-1Mo. In these cases, the coating was only slightly consumed by oxidation and the growth of the oxidation scale was greatly lowered by the presence of the coating. The same coating was able to grant protection from oxidation of Ti-48Al-2Nb-0.7Cr-0.3Si only for a limited period instead, since after 200 cycles the coating suffered complete oxidation. The lack of coating effectiveness observed in this last case (RNT protection) was tentatively attributed to diffusion phenomena that changed its composition.

Declaration of Competing Interest

The authors declare that they have no known competing financial interests or personal relationships that could have appeared to influence the work reported in this paper.

References

[1] E.A. Loria, Gamma titanium aluminides as prospective structural materials, Intermetallics 8 (2000) 1339–1345, https://doi.org/10.1016/S0966-9795(00)00073-X.

[2] K. Kothari, R. Radhakrishnan, N.M. Wereley, Advances in gamma titanium aluminides and their manufacturing techniques, Prog. Aerosp. Sci. 55 (2012) 1–16, https://doi.org/10.1016/j.paerosci.2012.04.001.

[3] H. Clemens, S. Mayer, Intermetallic titanium aluminides in aerospace applications – processing, microstructure and properties, Mater. High Temp. 33 (2016) 560–570, https://doi.org/10.1080/09603409.2016.1163792.

[4] B.P. Bewlay, S. Nag, A. Suzuki, M.J. Weimer, TiAl alloys in commercial aircraft engines, Mater. High Temp. 33 (2016) 549–559, https://doi.org/10.1080/09603409.2016.1183068.

[5] Y.-W. Kim, D.M. Dimiduk, Progress in the understanding of gamma titanium aluminides, JOM. 43 (1991) 40–47. https://doi.org/https://doi.org/10.1007/BF03221103.

[6] T. Tetsui, Gamma Ti aluminides for non-aerospace applications, Curr. Opin. Solid State Mater. Sci. 4 (1999) 243–248, https://doi.org/10.1016/S1359-0286(99)00023-6.

[7] J. Dai, J. Zhu, C. Chen, F. Weng, High temperature oxidation behavior and research status of modifications on improving high temperature oxidation resistance of titanium alloys and titanium aluminides: A review, J. Alloy. Compd. 685 (2016) 784–798, https://doi.org/10.1016/j.jallcom.2016.06.212.

[8] D. Kim, D. Seo, X. Huang, T. Sawatzky, H. Saari, J. Hong, Y.W. Kim, Oxidation behaviour of gamma titanium aluminides with or without protective coatings, Int. Mater. Rev. 59 (2014) 297–325, https://doi.org/10.1179/1743280414Y.0000000034.

[9] Y. Shida, H. Anada, Role of W, Mo, Nb and Si in oxidation of TiAl in air at high temperature, Nippon Kinzoku Gakkaishi/J. Jpn. Inst. Metals 58 (1994) 754–762.

[10] O. Ostrovskaya, C. Badini, G. Baudana, E. Padovano, S. Biamino, Thermogravimetric investigation on oxidation kinetics of complex Ti-Al alloys, Intermetallics (2017) 1–7, https://doi.org/10.1016/j.intermet.2017.09.020.

[11] A. Sobolev, A. Kossenko, K. Borodianskiy, Study of the effect of current pulse frequency on Ti-6Al-4V alloy coating formation by micro arc oxidation, Materials. 12 (2019) 3983-undefined. https://doi.org/10.3390/ma12233983.

[12] A. Sobolev, M. Zinigrad, K. Borodianskiy, Ceramic coating on Ti-6Al-4V by plasma electrolytic oxidation in molten salt: Development and characterization, Surf. Coat. Technol. 408 (2021), https://doi.org/10.1016/j.surfcoat.2021.126847.

[13] R. Pflumm, S. Friedle, M. Schütze, Oxidation protection of γ-TiAl-based alloys - A review, Intermetallics 56 (2015) 1–14, https://doi.org/10.1016/j.intermet.2014.08.002.

[14] Y. Xiong, S. Zhu, F. Wang, The oxidation behavior and mechanical performance of Ti60 alloy with enamel coating, Surf. Coat. Technol. 190 (2005) 195–199, https://doi.org/10.1016/j.surfcoat.2004.09.005.

[15] N. Laska, R. Braun, S. Knittel, Oxidation behavior of protective Ti-Al-Cr based coatings applied on the γ-TiAl alloys Ti-48-2-2 and TNM-B1, Surf. Coat. Technol. 349 (2018) 347–356, https://doi.org/10.1016/j.surfcoat.2018.05.067.

[16] R. Braun, N. Laska, S. Knittel, U. Schulz, Effect of intermetallic coatings on the tensile properties of a γ-TiAl based TNM alloy, Mater. Sci. Eng. A 699 (2017) 118–127, https://doi.org/10.1016/j.msea.2017.05.077.

[17] C.L.M. Frolich, E. Ebach-Stahl, R. Baun, No Title, Mat Wiss u Werkst. 38 (2007) 667–673.

[18] N. Laska, P. Watermeyer, L. Koliotassis, R. Braun, Oxidation behaviour of an intermetallic Ti–Al–Cr–Zr bond coat on a γ–TiAl based TNB alloy with 7YSZ thermal barrier coating, Mater. High Temp. 35 (2018) 187–194, https://doi.org/10.1080/09603409.2017.1404691.

[19] C. Badini, S.M. Deambrosis, E. Padovano, M. Fabrizio, O. Ostrovskaya, E. Miorin, G.C. D'Amico, F. Montagner, S. Biamino, V. Zin, Thermal shock and oxidation behavior of HiPIMS TiAlN coatings grown on Ti-48Al-2Cr-2Nb intermetallic alloy, Materials. 9 (2016) 961–983, https://doi.org/10.3390/ma9120961.

[20] C. Badini, S.M. Deambrosis, O. Ostrovskaya, V. Zin, E. Padovano, E. Miorin, Cyclic oxidation in burner rig of TiAlN coating deposited on Ti-48Al-2Cr- 2Nb by reactive HiPIMS, Ceram. Int. 43 (2017) 5417–5426, https://doi.org/10.1016/j.ceramint.2017.01.031.

[21] N. Cinca, J.M. Guilemany, Thermal spraying of transition metal aluminides: An overview, Intermetallics 24 (2012) 60–72, https://doi.org/10.1016/j.intermet.2012.01.020.

[22] H.L. Du, P.K. Datta, D. Griffin, A. Aljarany, J.S. Burnell-Gray, Oxidation and Sulfidation Behavior of AlTiN-Coated Ti–46.7Al–1.9W–0.5Si Intermetallic with CrN and NbN Diffusion Barriers at 850°C, Oxid. Met. 60 (2003) 29–46, https://doi.org/10.1023/A:1024613212818.

[23] S. Gong, H. Xu, Q. Yu, C. Zhou, Oxidation behaviour of TiAl/TiAl-SiC gradient coatings on gamma titanium aluminides, Surface Coat. Technol. 130 (2000) 128–132.

[24] V. Gauthier, F. Dettenwanger, M. Schütze, V. Shemet, W.J. Quadakkers, Oxidation-resistant aluminide coatings on γ-TiAl, Oxid. Met. 59 (2003) 233–255.

[25] A.R. Shugurov, M.S. Kazachenok, Mechanical properties and tribological behavior of magnetron sputtered TiAlN/TiAl multilayer coatings, Surf. Coat. Technol. (2018), https://doi.org/10.1016/j.surfcoat.2018.09.001.

[26] S.M. Deambrosis, F. Montagner, V. Zin, M. Fabrizio, C. Badini, E. Padovano, M. Sebastiani, E. Bemporad, K. Brunelli, E. Miorin, Ti1−xAlxN coatings by Reactive High Power Impulse Magnetron Sputtering: film/substrate interface effect on residual stress and high temperature oxidation, Surf. Coat. Technol. 354 (2018) 56–65, https://doi.org/10.1016/J.SURFCOAT.2018.09.004.

[27] M. Bartosik, D. Holec, D. Apel, M. Klaus, C. Genzel, J. Keckes, M. Arndt, P. Polcik, C.M. Koller, P.H. Mayrhofer, Thermal expansion of Ti-Al-N and Cr-Al-N coatings, Scr. Mater. 127 (2017) 182–185, https://doi.org/10.1016/j.scriptamat.2016.09.022.

[28] W.J. Zhang, B.v. Reddy, S.C. Deevi, Physical properties of TiAl-base alloys, Scr. Mater. 45 (2001) 645–651. 10.1016/S1359-6462(01)01075-2.

[29] D. Lundin, T. Minea, J.T. Gudmundsson, Preface, in: D. Lundin, T. Minea, J.T. Gudmundsson (Eds.), High Power Impulse Magnetron Sputtering Fundamentals, Technologies, Challenges and Applications, Elsevier, 2020: pp. xiii–xiv. https://doi.org/https://doi.org/10.1016/C2016-0-02463-4.

[30] M. Terner, S. Biamino, P. Epicoco, A. Penna, O. Hedin, S. Sabbadini, P. Fino, M. Pavese, U. Ackelid, P. Gennaro, F. Pelissero, C. Badini, Electron Beam Melting of High Niobium Containing TiAl Alloy: Feasibility Investigation, Steel Res. Int. 83 (2012) 943–949, https://doi.org/10.1002/srin.201100282.

[31] G. Baudana, S. Biamino, B. Klöden, A. Kirchner, T. Weißgärber, B. Kieback, M. Pavese, D. Ugues, P. Fino, C. Badini, Electron Beam Melting of Ti-48Al-2Nb-0.7Cr-0.3Si: Feasibility investigation, Intermetallics 73 (2016) 43–49, https://doi.org/10.1016/j.intermet.2016.03.001.

[32] S. Inamura, K. Nobugai, F. Kanamaru, The preparation of NaCl-type Ti1-xAlxN solid solution, J. Solid State Chem. 68 (1987) 124–127, https://doi.org/10.1016/0022-4596(87)90293-3.

[33] T. Ikeda, H. Satoh, Phase formation and characterization of hard coatings in the Ti-Al-N system prepared by the cathodic arc ion plating method, Thin Solid Films 195 (1991) 99–110, https://doi.org/10.1016/0040-6090(91)90262-V.

[34] L. Ipaz, W. Aperador, J. Caicedo, J. Esteve, G. Zambrano, A Practical Application of X-Ray Spectroscopy in Ti-Al-N and Cr-Al-N Thin Films, in: S.K. Sharma (Ed.), X-Ray Spectroscopy, InTech, 2010, p. 280. https://doi.org/10.5772/29640.

[35] J.P. Zhao, X. Wang, T.S. Shi, X.H. Liu, Evolution of the texture of TiN films prepared by fittered arc deposition, J. Appl. Phys. 79 (1996) 9399–9401, https://doi.org/10.1063/1.362576.

[36] J.T. Chen, J. Wang, F. Zhang, G.A. Zhang, X.Y. Fan, Z.G. Wu, P.X. Yan, Characterization and temperature controlling property of TiAlN coatings deposited by reactive magnetron co-sputtering, J. Alloy. Compd. 472 (2009) 91–96.

[37] H. Yue, Y. Chen, X. Wang, F. Kong, Effect of beam current on microstructure, phase, grain characteristic and mechanical properties of Ti-47Al-2Cr-2Nb alloy fabricated by selective electron beam melting, J. Alloy. Compd. 750 (2018) 617–625, https://doi.org/10.1016/j.jallcom.2018.03.343.

[38] F. Jose, R. Ramaseshan, P.K. Parida, A. Dasgupta, A.K. Balamurugan, S. Dash, A.K. Tyagi, Structural and Nano-mechanical characterization of TiN/Ti1-xAlxN multilayered Thin Films, IEEE (2011) 562–566.

[39] M.D. Banus, T.B. Reed, A.J. Strauss, Electrical and magnetic properties of TiO and VO, Phys. Rev. Lett. B. 5 (1972) 2775–2784.

[40] J.F. Marco, J.R. Gancedo, M.A. Auger, O. Sánchez, J.M. Albella, Chemical stability of TiN, TiAlN and AlN layers in aggressive SO2 environments, Surf. Interface Anal. 37 (2005) 1082–1091, https://doi.org/10.1002/sia.2083.

[41] M. Mitoraj, E. Godlewska, O. Heintz, N. Geoffroy, S. Fontana, S. Chevalier, Scale composition and oxidation mechanism of the Ti-46Al-8Nb alloy in air at 700 and 800 °C, Intermetallics 19 (2011) 39–47, https://doi.org/10.1016/j.intermet.2010.09.006.

[42] H. Anada, Y. Shida, Effect of Mo addition on the oxidation behaviour of TiAl intermetallic compound, Mater. Trans., JIM 36 (1995) 533–539.

[43] J.W. Fergus, Review of the effect of alloy composition on the growth rates of scales formed during oxidation of gamma titanium aluminide alloys, Mater. Sci. Eng., A 338 (2002) 108–125, https://doi.org/10.1016/S0921-5093(02)00064-3.

[44] M. Baben, M. Hans, D. Primetzhofer, S. Evertz, H. Ruess, J.M. Schneider, Unprecedented thermal stability of inherently metastable titanium aluminum nitride by point defect engineering, Mater. Res. Lett. 5 (2017) 158–169, https://doi.org/10.1080/21663831.2016.1233914.

[45] M.T. Baben, L. Raumann, D. Music, J.M. Schneider, Origin of the nitrogen over- and understoichiometry in Ti0.5Al0.5N thin films, J. Phys.: Condens. Matter 24 (2012).

[46] N. Jiang, Y.G. Shen, H.J. Zhang, S.N. Bao, X.Y. Hou, Superhard nanocomposite Ti-Al-Si-N films deposited by reactive unbalanced magnetron sputtering, Mater. Sci. Eng. B: Solid-State Mater. Adv. Technol. B 135 (2006) 1–9, https://doi.org/10.1016/j.mseb.2006.06.043.

[47] Y.X. Xu, H. Riedl, D. Holec, L. Chen, Y. Du, P.H. Mayrhofer, Thermal stability and oxidation resistance of sputtered Ti-Al-Cr-N hard coatings, Surf. Coat. Technol. 324 (2017) 48–56, https://doi.org/10.1016/j.surfcoat.2017.05.053.

[48] D. Yu, C. Wang, X. Cheng, F. Zhang, Microstructure and properties of TiAlSiN coatings prepared by hybrid PVD technology, Thin Solid Films 517 (2009) 4950–4955, https://doi.org/10.1016/j.tsf.2009.03.091.

[49] F. Pei, H.J. Liu, L. Chen, Y.X. Xu, Y. Du, Improved properties of TiAlN coating by combined Si-addition and multilayer architecture, J. Alloy. Compd. 790 (2019) 909–916, https://doi.org/10.1016/j.jallcom.2019.03.248.

[50] A. Flink, J.M. Andersson, B. Alling, R. Daniel, J. Sjölén, L. Karlsson, L. Hultman, Structure and thermal stability of arc evaporated (Ti0.33Al0.67)1 - xSixN thin films, Thin Solid Films 517 (2008) 714–721, https://doi.org/10.1016/j.tsf.2008.08.126.

[51] C. Saringer, M. Tkadletz, A. Stark, N. Schell, C. Czettl, N. Schalk, In-situ investigation of the oxidation behavior of metastable CVD-Ti1-xAlxN using a novel combination of synchrotron radiation XRD and DSC, Surf. Coat. Technol. 374 (2019) 617–624, https://doi.org/10.1016/j.surfcoat.2019.05.072.